Fibers and Polymers 2002, Vol.3, No.4, 159-168

Processing of Polyurethane/Polystyrene Hybrid Foam and Numerical Simulation

Won Ho Lee, Seok Won Lee, Tae Jin Kang, Kwansoo Chung, and Jae Ryoun Youn*

School of Materials Science and Engineering, Seoul National University, Seoul 151-742, Korea
(Received August 27, 2002; Revised October 30, 2002; Accepted November 19, 2002)

Abstract: Polyurethane foams were produced by using a homogenizer as a mixing equipment. Effects of stirring speed on the foam structure were investigated with SEM observations. Variation of the bubble size, density of the foam, compressive strength, and thermal conductivity were studied. A hybrid foam consisting of polyurethane foam and commercial polystyrene foam is produced. Mechanical and thermal properties of the hybrid foam were compared with those of pure polyurethane foam. Advancement of flow front during mold filling was observed by using a digital camcorder. Four types of mold geometry were used for mold filling experiments. Flow during mold filling was analyzed by using a two-dimensional control volume finite element method. Variation of foam density with respect to time was experimentally measured. Creeping flow, uniform density, uniform conversion, and uniform temperature were assumed for the numerical simulation. It was assumed for the numerical analysis that the cavity has thin planar geometry and the viscosity is constant. The theoretical predictions were compared with the experimental results and showed good agreement.

Keywords: Polyurethane, Polystyrene, Hybrid foam, Mold filling, Control volume finite element method

Introduction

Reaction Injection Molding (RIM) is a processing method for rapid production of complex plastic parts directly from low viscosity monomers or reactive oligomers injected into a mold[1]. Since the 1970s, during which special high-pressure equipment for efficient mixing of the reactants was proposed, RIM technology has been widely used for polymer processing, especially in the automotive industry[2].

A schematic diagram of the reaction injection molding process is shown in Figure 1. In the RIM process, two or more low viscosity liquid streams, which become reactive when brought together, are mixed in the mixing head by utilizing turbulent mixing prior to being injected into the mold where they are polymerized and solidified[3]. Polyurethane, the most frequently used system for RIM, has various characteristics according to the composition of monomers or formation of oligomers. Polyurethane foam, used for thermal insulation of home appliances, is produced by reaction injection molding (RIM) with blowing agents that have been mixed with the polyurethane resin in advance[3,4]. Polyol and isocyanate are required monomers that are mixed along with other additives, such as catalysts, surfactants, and blowing agents. Polyurethane foam generally has low mechanical properties but has many advantages such as weight reduction, savings of materials, increase in impact strength, improvement of sound and thermal insulation[5].

In order to obtain final products of improved physical properties, polymers are often processed with the addition of various kinds of fillers or reinforcing materials such as chopped fibers, flakes and continuous fibers. They are added to one of reactants for the RRIM (Reinforcement Reaction Injection Molding) process or reinforcing materials are placed into the mold before injecting the reactive mixture for the SRIM (Structural Reaction Injection Molding) process [6,7]. The main objectives of the reinforcement are improvement in dimensional stability and mechanical properties.

In this study, commercial polystyrene foams were placed in the mold before injection of the polyurethane resin to produce the hybrid foam. Thermal conductivity and compressive strength of pure polyurethane foams which were produced at different stirring speed were compared with the properties of the hybrid foam. Mold filling of polyurethane foam was observed by experiment, and theoretical modeling was performed for cavity filling.

*Corresponding author: jaeryoun@gong.snu.ac.kr

Experimental

Materials

Table 1 lists polyol and MDI used in the experiment. Commercial polystyrene foam beads with the average diameter of 12 mm were obtained and used as the insert in the mold. Some physical properties of the polystyrene foam are given in Table 2.

Table 1. Materials used in the experiment

Isocyanate	MDI(4,4'diphenylmethane diisocyanate)
Polyol	Propylene oxide based diols
Polyol mixture	Polyol (100 wt%) + Silicon surfactant (2.0 wt%) + Catalyst (1.7%) + Blowing Agent
Blowing agent	Physical blowing agent : dichlorofluoroethane Chemical blowing agent : H_2O

Table 2. Physical properties of commercial polystyrene foams

Geometry	Density (g/cm^3)	Porosity	Thermal conductivity (W/m·K)
Sphere (12 mm diameter)	0.042	0.45	0.036

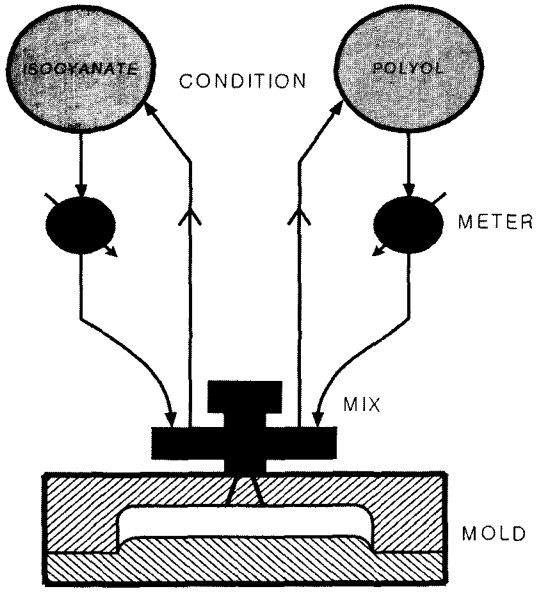

Figure 1. Schematic diagram of the reaction injection molding process.

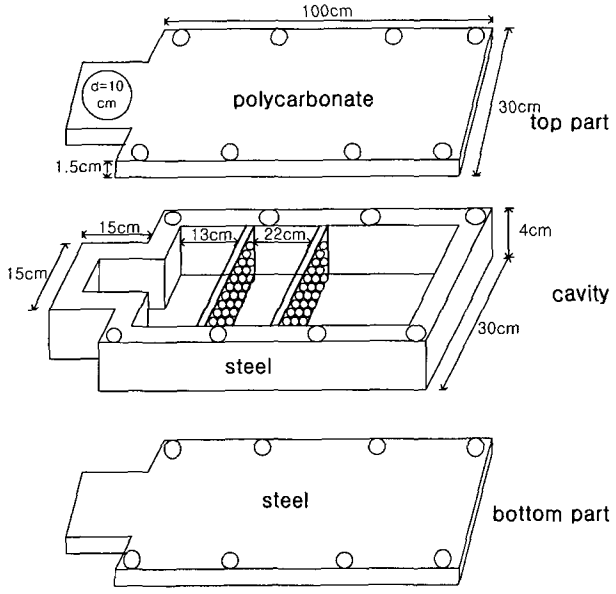

Figure 2. Schematic diagram of the mold used in the experiment.

Processing of Polyurethane

The polyol was mixed with the stoichiometric amount of

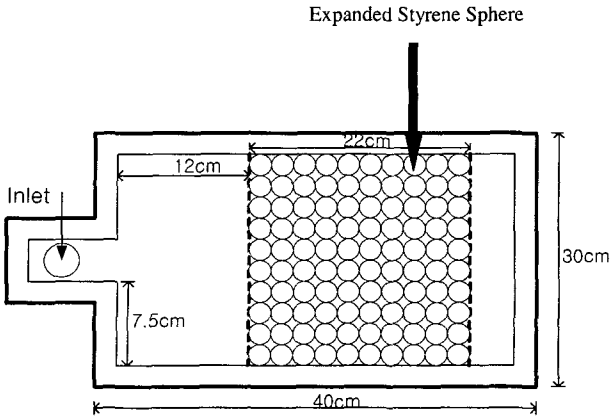

Figure 3. Mold geometry for producing the hybrid foam.

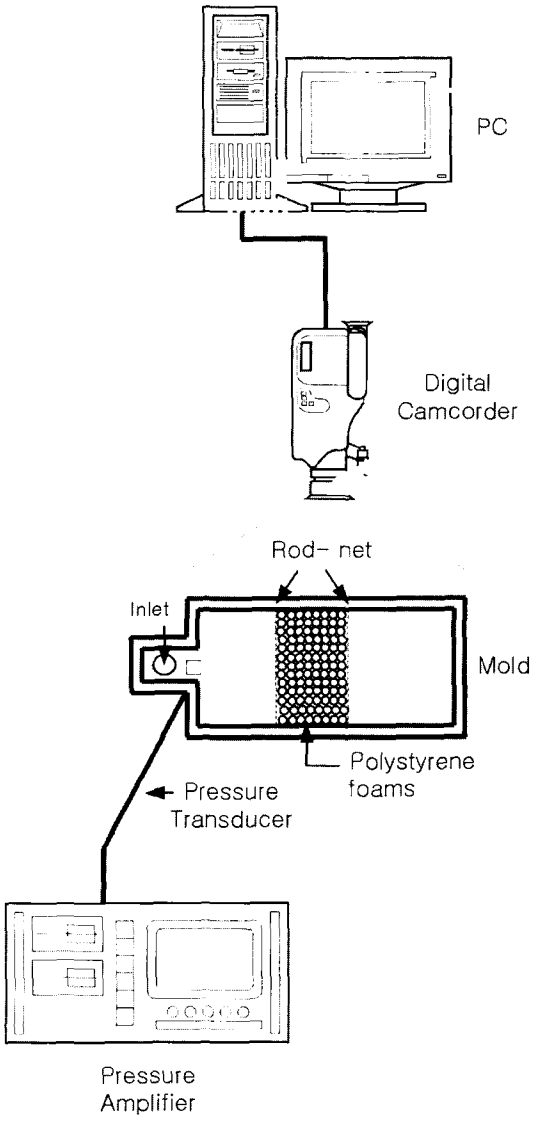

Figure 4. Schematic diagram of the experimental setup for observation of the mold filling.

isocyanate in a polyethylene cup using the homogenizer. The mixing was carried out for about 20 seconds at a various stirring speed of 6000, 8000, 10000, and 12000 rpm. The mixed reactants were immediately poured into the mold, and then the blowing agent dissolved in the polyol yielded gas to form bubbles in the polyurethane. Finally, polyurethane foams are obtained with respect to various stirring speeds. The mold used in this study is shown in Figure 2. Dimensions of the end gated rectangular mold cavity are 100 cm (length) ×30 cm (width)×4 cm (thickness). For samples obtained in each experiment, density, thermal conductivity, and compressive strength are measured. Thermal conductivity was measured by using a heat flow metering instrument (HC-074) supplied from EKO Instruments Trading.

Processing of Hybrid Foam

Hybrid foams consist of two different foamed materials. Figure 3 shows the installation of the mold and the experimental procedure is as follows. After a mold release agent was applied to the entire mold surface, the rod-net was located inside the mold and polystyrene foams were placed inside the installed rod-net area. Then, the polyurethane mixture, which was mixed by using a homogenizer, was poured into the mold. At the early stage, polyurethane foam filled the free space by self - expansion which is induced by bubble growth. After filling all the free space, polyurethane foam began to penetrate through the pre-filled polystyrene beads and polyurethane foam filled all the spaces between the polystyrene foams. At last, hybrid foam consisting of expanded PS beads and polyurethane was produced.

Mold Filling

Advancement of the flow front during mold filling was observed by using a digital camcorder as shown in Figure 4. Motion and still pictures were obtained to determine the flow patterns during the entire mold filling. Mold cavity pressure was also measured with the aid of pressure transducer which was mounted at the end of the gate. The experiments were carried out by utilizing different mold types of 4 kinds as shown in Figure 5.

Numerical Analysis

Governing Equation

In order to numerically analyze the polyurethane flow in two-dimensional rectangular mold, the following assumptions were made.

(1) Two-dimensional thin cavity.
(2) Creeping flow.
(3) Uniform density.
(4) Uniform conversion.
(5) Uniform temperature.

From the above assumptions, continuity and momentum equations are derived as follows:

$$\frac{\partial \rho}{\partial t} + \rho\frac{\partial u}{\partial x} + \rho\frac{\partial v}{\partial y} = 0 \tag{1}$$

$$0 = -\frac{\partial p}{\partial x} + \frac{\partial}{\partial z}\left(\eta\frac{\partial u}{\partial z}\right) \tag{2}$$

$$0 = -\frac{\partial p}{\partial y} + \frac{\partial}{\partial z}\left(\eta\frac{\partial v}{\partial z}\right) \tag{3}$$

where ρ is the density, η the viscosity, p pressure, u and v are the velocity components in the x and y direction.

Boundary conditions are shown below.

$$u = v = 0, \qquad \text{at} \qquad z = h$$

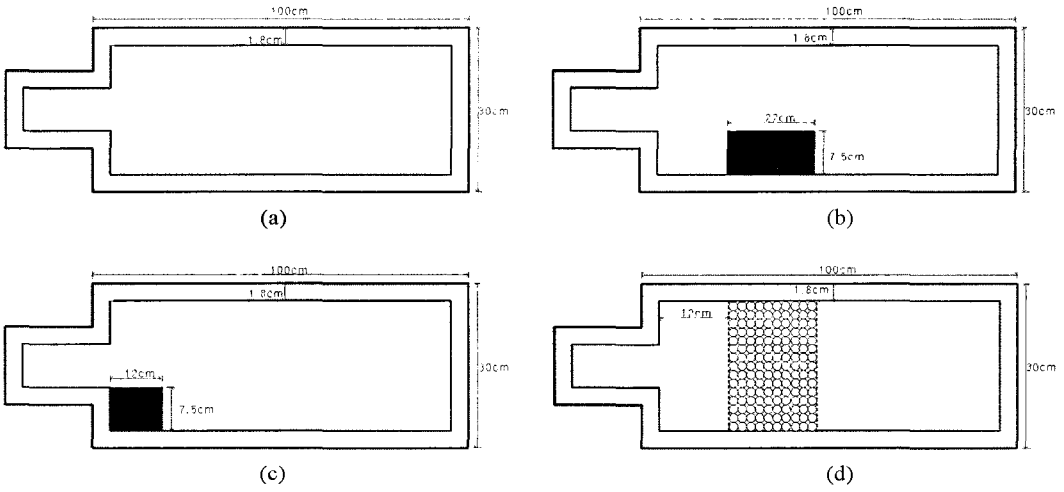

Figure 5. Schematic diagram of the mold; (a) without any block, (b) with a block at the lower left corner, (c) with a block at the bottom, (d) with expanded polystyrene beads in the rod-net.

$$\frac{\partial u}{\partial z} = \frac{\partial v}{\partial z} = 0, \quad \text{at} \quad z = 0$$

Equation (2) can be integrated in the thickness (z) direction.

$$\frac{\partial u}{\partial z} = \frac{z}{\eta}\frac{\partial p}{\partial x} \tag{4}$$

Velocity can be found by the integration of equation (4) in the thickness (z) direction.

$$u = -\frac{(h^2 - z^2)}{2\eta}\frac{\partial p}{\partial x} \tag{5}$$

Average velocity can be obtained as shown below.

$$\bar{u} = \frac{1}{h}\int_0^h u\,dz = -\frac{1}{2\eta h}\frac{\partial p}{\partial x}\int_0^h (h^2 - z^2)\,dz = -\frac{h^2}{3\eta}\frac{\partial p}{\partial x} \tag{6}$$

Similarly, velocity in the y-direction, v, can be obtained as below.

$$\bar{v} = \frac{1}{h}\int_0^h v\,dz = -\frac{1}{2\eta h}\frac{\partial p}{\partial y}\int_0^h (h^2 - z^2)\,dz = -\frac{h^2}{3\eta}\frac{\partial p}{\partial y} \tag{7}$$

Besides, Darcy's law can be applied to the porous media

$$\bar{u} = -\frac{K}{\eta}\frac{\partial p}{\partial x} \tag{8}$$

$$\bar{v} = -\frac{K}{\eta}\frac{\partial p}{\partial y} \tag{9}$$

Thus, average velocity vectors can be rewritten as below.

$$\bar{u} = -\frac{K^*}{\eta}\frac{\partial p}{\partial x} \tag{10}$$

$$\bar{v} = -\frac{K^*}{\eta}\frac{\partial p}{\partial y} \tag{11}$$

$$K^* \begin{cases} = \dfrac{h^2}{3} & \text{if without porous media} \\ = K & \text{if with porous media} \end{cases}$$

After integration of equation (1), the following relations can be derived.

$$\frac{\partial \ln\rho}{\partial t} + \frac{\partial u}{\partial x} + \frac{\partial v}{\partial y} = 0$$

$$\int_0^h \frac{d\ln\rho}{\partial t}dz + \frac{\partial}{\partial x}\left(\int_0^h u\,dz\right) + \frac{\partial}{\partial y}\left(\int_0^h v\,dz\right) = 0$$

$$\frac{\partial \ln\rho}{\partial t} + \frac{\partial}{\partial x}\left(\frac{1}{h}\int_0^h u\,dz\right) + \frac{\partial}{\partial y}\left(\frac{1}{h}\int_0^h v\,dz\right) = 0$$

$$\frac{\partial \ln\rho}{\partial t} + \frac{\partial}{\partial x}(\bar{u}) + \frac{\partial}{\partial y}(\bar{v}) = 0 \tag{12}$$

Substitution of equations (10) and (11) into equation (12) yields the final pressure equation as below.

$$\frac{\partial \ln\rho}{\partial t} - \frac{\partial}{\partial x}\left(\frac{K^*}{\eta}\frac{\partial p}{\partial x}\right) - \frac{\partial}{\partial y}\left(\frac{K^*}{\eta}\frac{\partial p}{\partial y}\right) = 0 \tag{13}$$

where K is the permeability of porous media, h the thickness in the z direction, $\bar{u}$ and $\bar{v}$ the average velocity components in the x and y direction. The viscosity is assumed constant in this study and the viscosity measured by Kim and Youn[4] is used ($h_o = 53.07$ Pa·s).

Numerical Formulation

Governing equation for pressure can be solved by the control volume finite element method (CVFEM). In the control volume finite element method[8-10], pressure field is determined in order to satisfy the conservation law, which is evaluated from the flux across the control-volume boundary. Figure 6 shows finite elements and their definition of control volume. The sub-control volume surrounding a given vertex includes one-third of each area of six primary triangular elements sharing the vertex, so that each triangle of area A is divided into three equal quadrilateral areas of $A/3$.

Boundary conditions for equation (13) are as below.

at C_m $\quad p = 0$

at C_i or C_o $\quad \dfrac{\partial p}{\partial n} = 0$

where n denotes the outward normal direction. Equation (14) is derived from equation (13) as follows.

$$\frac{\partial}{\partial x}\left(\frac{K^*}{\eta}\frac{\partial p}{\partial x}\right) + \frac{\partial}{\partial y}\left(\frac{K^*}{\eta}\frac{\partial p}{\partial y}\right) = \frac{\partial \ln\rho}{\partial t}$$

$$\nabla \cdot \left(\frac{K^*}{\eta}\nabla p\right) = \frac{\partial \ln\rho}{\partial t}$$

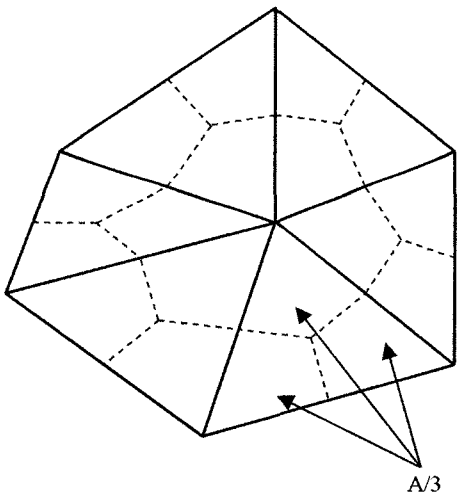

Figure 6. Triangular finite elements and definition of control volume.

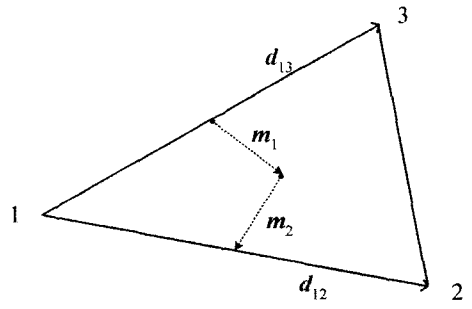

Figure 7. Triangular element and vectors used in pressure calculation.

$$\iint_A \nabla \cdot \left(\frac{K^*}{\eta}\nabla p\right) dA = \iint_A \frac{\partial \ln \rho}{\partial t} dA$$

$$\int_S \frac{K^*}{\eta}\nabla p \cdot \boldsymbol{n} dS = \iint_A \frac{\partial \ln \rho}{\partial t} dA$$

$$\sum_e \frac{K^{*e}}{\eta^e}\int_{S^e} \nabla p \cdot \boldsymbol{n} dS^e = \sum_e \iint_{A^e} \frac{\partial \ln \rho}{\partial t} dA^e$$

$$\sum_e \frac{K^{*e}}{\eta^e}\int_{S^e} \nabla p \cdot \boldsymbol{m} dS^e = \sum_e \frac{\partial \ln \rho}{\partial t}\frac{A^e}{3} \tag{14}$$

where subscript e represent an element, and A the area of each element.

Figure 7 shows vectors used in the pressure calculation. If the pressure is assumed to vary linearly in the element, the gradient of pressure can be expressed as below.

$$\nabla p = -\frac{(p_3 - p_1)\boldsymbol{d}_{12}^+ - (p_2 - p_1)\boldsymbol{d}_{13}^+}{2A_e} \tag{15}$$

where superscript + means that the vector is rotated clockwise by an angle $\pi/2$ along the plane. Let $\boldsymbol{m}$ be the vector that is normal to the boundary of sub-control volume and has the same length as the sub-control volume boundary. Then, the surface integration term of equation (14) can be evaluated using the relation below.

$$\boldsymbol{m} = -(\boldsymbol{m}_1^+ + \boldsymbol{m}_2^+) = -\frac{1}{2}(\boldsymbol{d}_{12}^+ - \boldsymbol{d}_{13}^+) = -\frac{1}{2}\boldsymbol{d}_{32}^+ \tag{16}$$

The relation of $\boldsymbol{a}^+ \cdot \boldsymbol{b}^+ = \boldsymbol{a} \cdot \boldsymbol{b}$ is used for the deviation of the above. From equations (14) and (16),

$$\sum_e \left\{\frac{K^*}{4A^e\eta^e}[p_3\boldsymbol{d}_{12} \cdot \boldsymbol{d}_{32} - p_2\boldsymbol{d}_{13} \cdot \boldsymbol{d}_{32} - p_1\boldsymbol{d}_{32} \cdot \boldsymbol{d}_{32}]\right\}$$

$$= \sum_e \frac{\partial \ln \rho}{\partial t}\frac{A^e}{3} \tag{17}$$

Substitution of equation (17) to (14) leads to the following equation.

$$p_1 = \frac{\sum_e B^e p_2^e + \sum_e C^e p_3^e + \sum_e D^e}{\sum_e A^e} \tag{18}$$

where

$$A^e = \frac{K^{*e}}{4A^e\eta^e}\left|\boldsymbol{d}_{32}^e\right|^2$$

$$B^e = -\frac{K^{*e}}{4A^e\eta^e}\boldsymbol{d}_{13}^e \cdot \boldsymbol{d}_{32}^e$$

$$C^e = \frac{K^{*e}}{4A^e\eta^e}\boldsymbol{d}_{12}^e \cdot \boldsymbol{d}_{32}^e$$

$$D^e = -\frac{\partial \ln \rho A^e}{\partial t}\frac{A^e}{3}$$

Node-by-node iterations make it possible to obtain the pressure field and neither stiffness matrix nor coordinate transformation is necessary[11].

Results and Discussion

Properties of Polyurethane and Hybrid Foams

Polyurethane foam was produced at various stirring speeds. Figure 8 shows SEM pictures of the foamed polyurethane samples. Measured properties of the samples are listed in Table 3. Mean diameter of the cells was measured by an image processing technique with respect to the mixing speed. It was found that faster stirring speed yielded smaller mean diameter of bubbles. Therefore, the

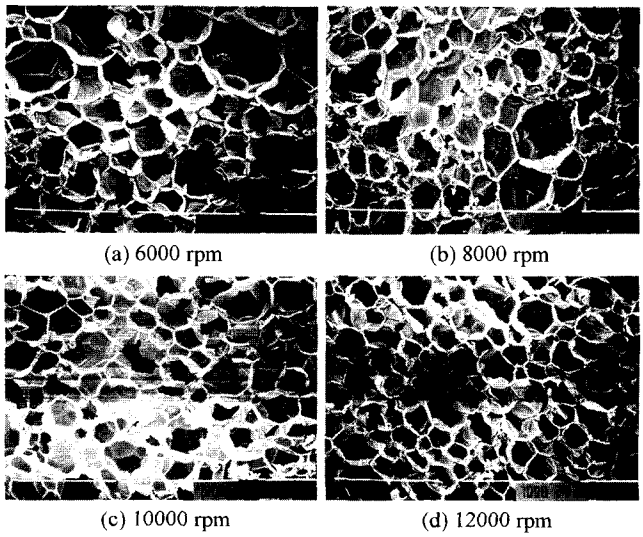

Figure 8. SEM pictures of the foamed polyurethane samples with respect to stirring speed.

Table 3. Measured properties of polyurethane foam for different stirring speed

Stirring speed	Mean diameter (μm)	Density (kg/m^3)	Cell density (10^{12}/m^3)	Thermal conductivity (W/m·K)	Compressive strength (MPa)
6000 rpm	332	31.9	1.42	0.0198	5.78
8000 rpm	273	32.6	2.36	0.0206	7.74
10000 rpm	217	35.4	4.66	0.0194	8.23
12000 rpm	194	38.4	6.73	0.0208	8.43
Hybrid foam		62.8		0.0311	43.02

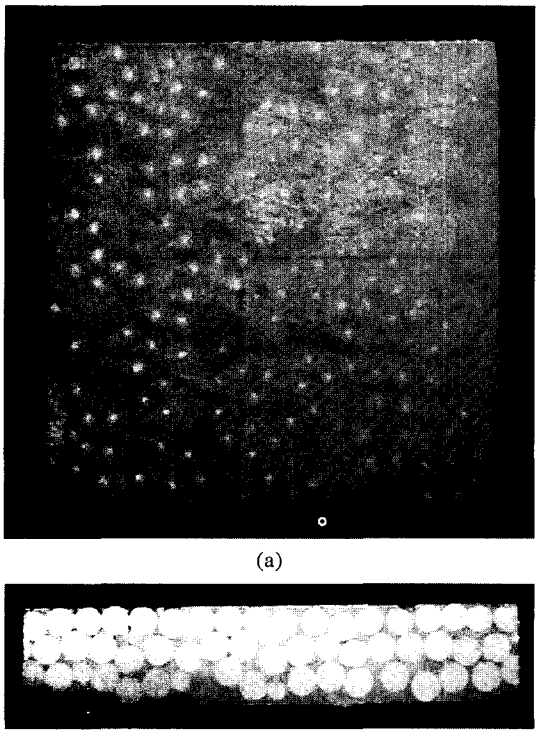

(a)

(b)

Figure 9. Hybrid foam samples; (a) Top view, (b) Cross-sectional view perpendicular to the flow direction.

stirring speed plays an important role in nucleation and growth of bubbles. Density of the foam and the number of cells were increased as the mixing speed was increased. Compressive strength of the polyurethane foam was increased with respect to the stirring speed as shown in Table 3. Thermal conductivity of the foam was slightly increased as the stirring speed was increased. If the density of the plastic foam is in the range of 30 to 80 kg/m^3, density is not an important parameter influencing the thermal conductivity[3]. Variation of the thermal conductivity is similar to that of the density. In this experiment, polyurethane foam produced at the speed of 12000 rpm was used when the hybrid foam was made. Compared with pure polyurethane foam, the compressive strength of hybrid foam is quite larger but

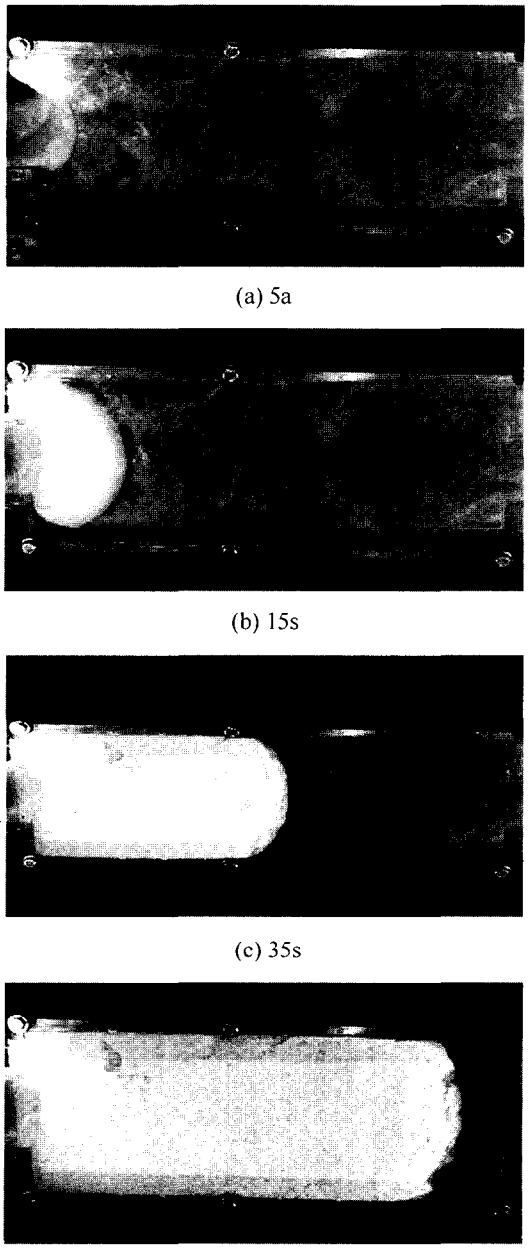

(a) 5a

(b) 15s

(c) 35s

(d) The end of filling

Figure 10. Advancement of the flow front without the block.

(a) 5s

(b) 15s

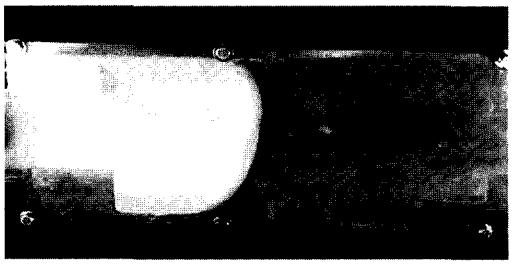

(c) 25s

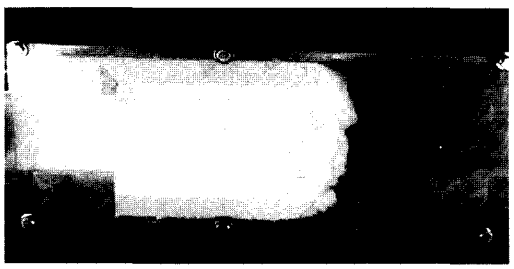

(d) The end of filling

'igure 11. Advancement of the flow front with the block at the left orner.

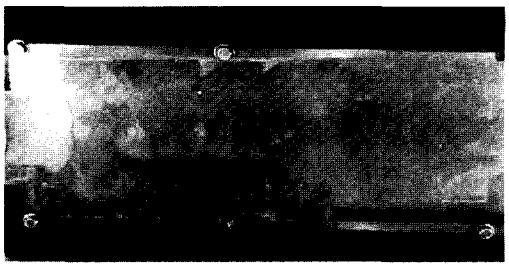

(a) 5s

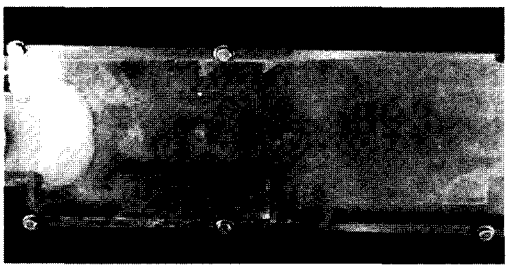

(b) 15s

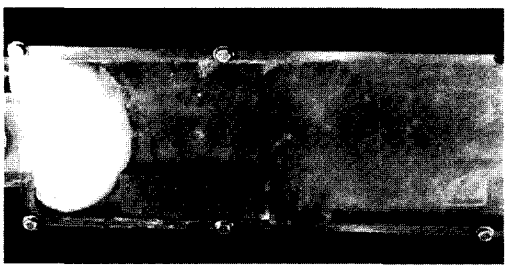

(c) 35s

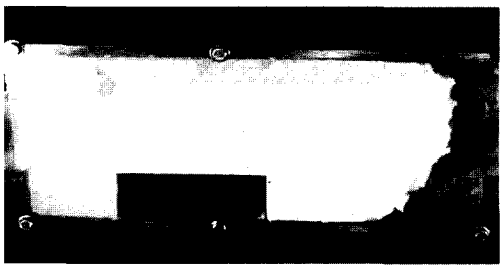

(d) The end of filling

Figure 12. Advancement of the flow front with the block at the bottom.

hermal conductivity of the hybrid foam is higher than that of the pure polyurethane foam. Figure 9 shows pictures of he hybrid foam sample.

Mold Filling

Mold filling behavior for each experiment is shown in Figures 10 to 13. In Figure 10, flow front of the polyurethane oam is radial near the gate and then rectilinear as the flow ront touches the cavity side walls. In the case of hybrid oam, polyurethane foam filled up the free space first. After filling all the free space, polyurethane foam began to penetrate through the compacted polystyrene beads and polyurethane foam filled all the gaps between the polystyrene beads as shown in Figure 13. Density change of a pure polyurethane foam was measured with respect to time, as plotted in Figure 14. An empirical equation for density variation is proposed as follows: $\rho = \rho_0 + A\exp(-Bt)$, ρ_0(g/cm^3) = 0.0396, A (g/cm^3) = 0.8226, B (s^{-1}) = 0.0835. In the early stage, as time increases, the density suddenly decreases. But, in the next stage, the density decreases slowly.

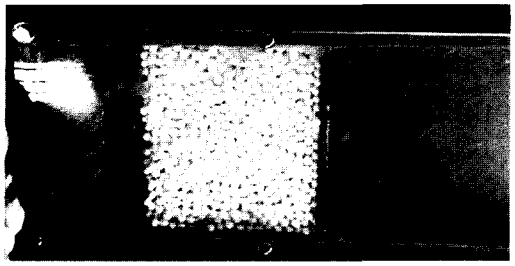

(a) 5s

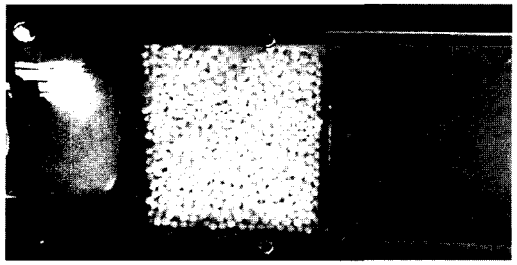

(b) 15s

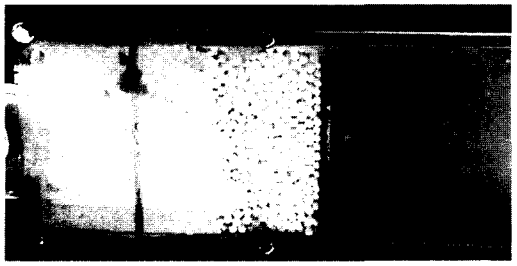

(c) 35s

(d) The end of filling

Figure 13. Advancement of the flow front through the polystyrene foams.

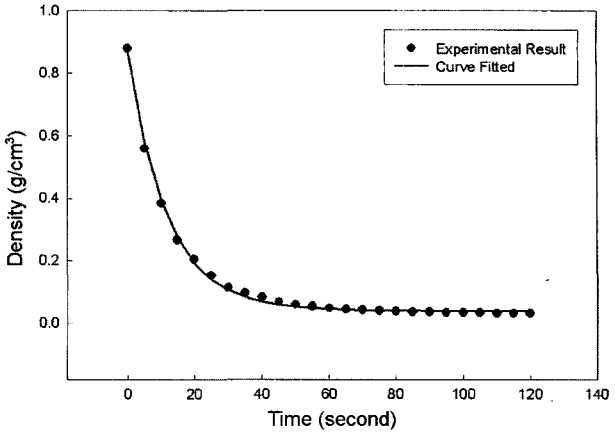

Figure 14. Density variation measured as a function of time.

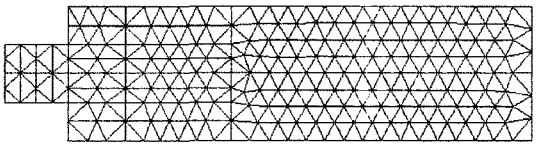

Figure 15. Two-dimensional finite element mesh used for the filling analysis without the block.

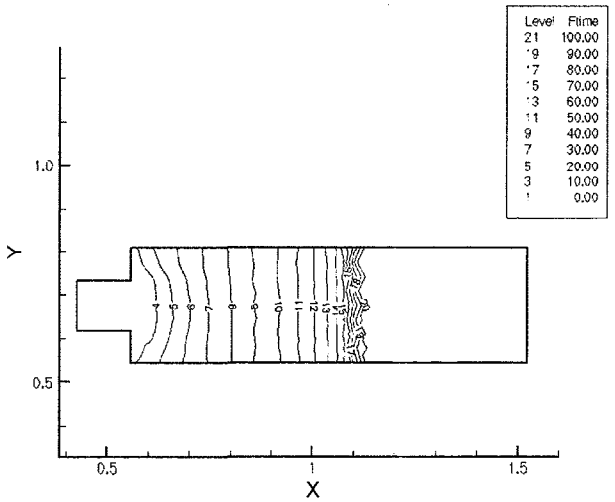

Figure 16. Flow front advancement with respect to time.

Comparison with Numerically Predicted Results

Numerical simulation was carried out for three different types of the mold. Figure 15 represents the finite element mesh for the end-gated rectangular mold cavity without any block. There are 239 nodes and 404 finite elements. Advancement of the fluid front predicted with respect to time is illustrated in Figure 16. In 100 seconds, two thirds of the mold is filled and the numerical calculation is terminated. Figure 17 shows the pressure distribution and the velocity vectors at the end of simulation. The maximum pressure is about 0.28 Pa, and the reference vector represents 1.0×10^{-7} m/s. The finite element mesh for the mold with a solid block at the lower left corner is presented in Figure 18. It has 233 nodes and 392 elements. Advancement of the fluid front predicted with respect to time is represented in Figure 19. Compared with the case of the mold without the block, filling time is a little longer. The pressure distribution and velocity vectors at the end of simulation are shown in Figure 20. The maximum pressure and the reference vector shown in Figure 21 are also much larger than those of the

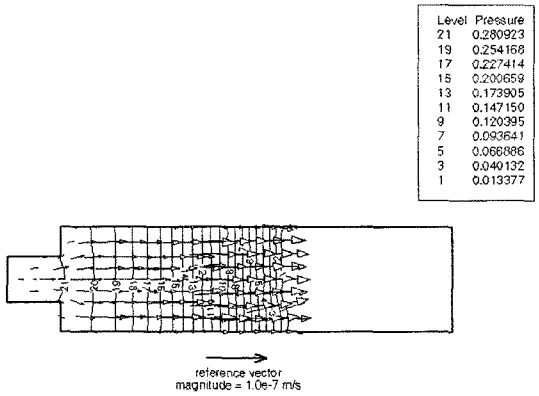

Figure 17. Pressure contours and velocity vectors at the end of filling.

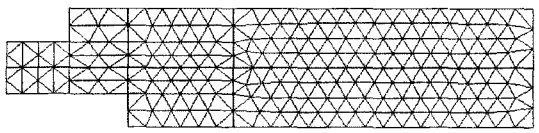

Figure 18. Two-dimensional finite element mesh used for the filling analysis with the block at the lower left corner.

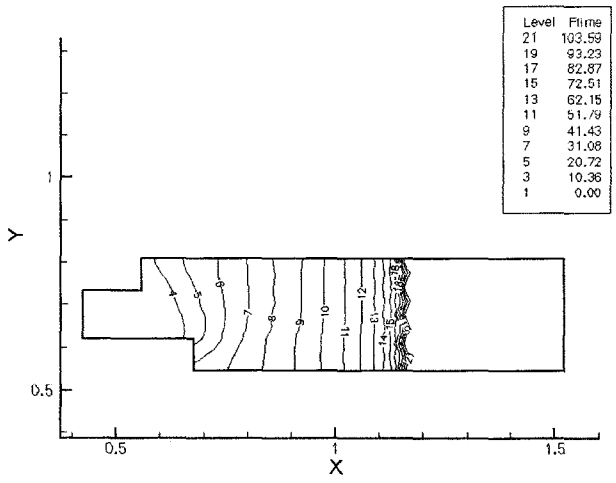

Figure 19. Flow front advancement with respect to time.

mold without the block. Lastly, finite element mesh of the mold with a solid block at the bottom is presented in Figure 21. There are 229 nodes and 380 elements. Fill time is the longest among three different molds as shown in Figure 22. Figure 23 represents the pressure distribution and the velocity vectors at the end of simulation. The maximum pressure and the reference vector are respectively about 0.19 MPa and 5×10^{-8} m/s.

As can be seen in the experiment, flow front is radial near the gate and then becomes rectilinear as the flow front touches the cavity side wall. Compared with experimental

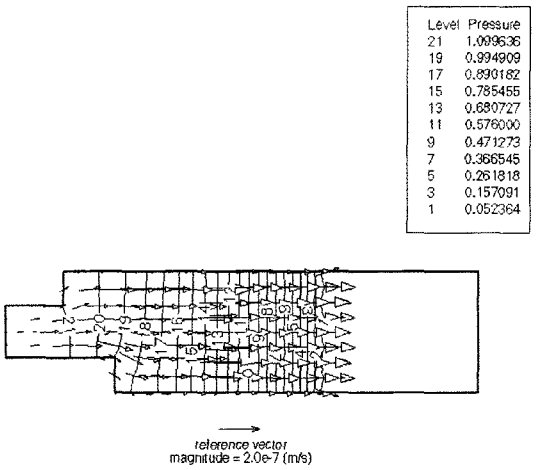

Figure 20. Pressure contours and velocity vectors at the end of filling.

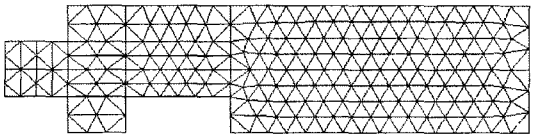

Figure 21. Two-dimensional finite element mesh used for the filling analysis with the block at the bottom.

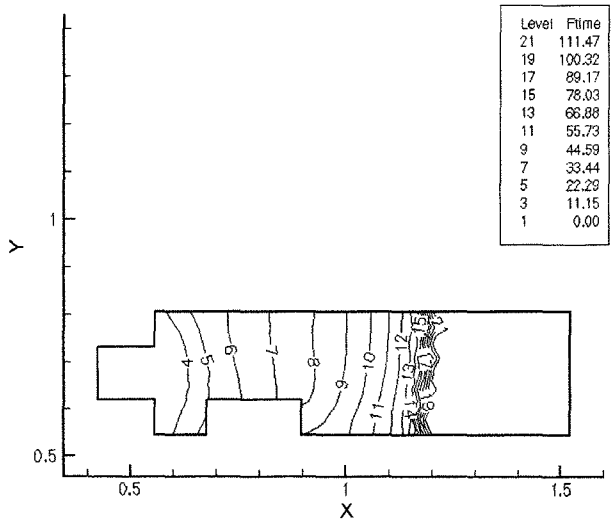

Figure 22. Flow front advancement with respect to time.

results, the predicted flow front shape and advancement are in good agreement.

Conclusions

Polyurethane foams were produced by using a homogenizer as a mixing equipment. Effects of processing conditions on

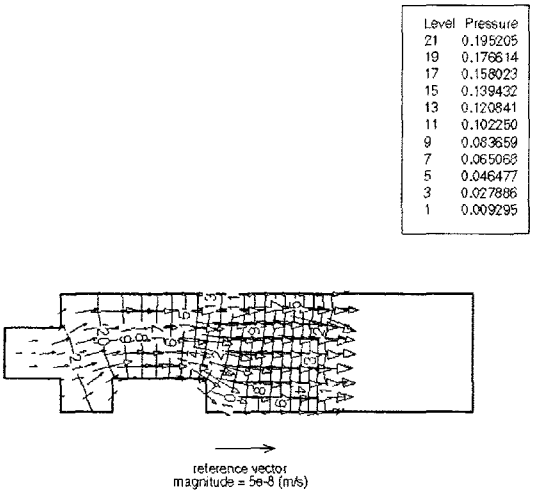

Figure 23. Pressure contours and velocity vectors at the end of filling.

the foam structure are studied with SEM observation. As the mixing speed is increased, the mean diameter is decreased but foam density, number of cells, and compressive strength are increased. Hybrid foam consisting of commercial polystyrene foam and polyurethane foam was made. Compared with pure polyurethane foam, compressive strength of the hybrid foam was much larger but thermal conductivity was higher. Mold filling of polyurethane foam was studied experimentally and numerically. In the experiment, advancement of the flow front during mold filling was observed by using a digital camcorder. Mold filling of the cavity by self-expansion of the polyurethane foam is predicted by a CVFEM simulation. Pressure based control volume finite element method is successfully applied to the moving boundary problem to predict the pressure and velocity variation with respect to time. The theoretical prediction showed good agreement with the experimental results for flow front advancement and fill time.

Acknowledgement

This study was supported by the Korea Science and Engineering Foundation (KOSEF) through the Applied Rheology Center (ARC), an official KOSEF-created engineering research center (ERC) at Korea University, Seoul, Korea.

References

1. C. W. Macosko, "RIM: Fundamentals of Reaction Injection Molding", Hanser Publisher, New York, 1989.
2. E. Y. Polushkin, O. M. Polushkina, A. Y. Malkin, V. G. Kulichikhin, W. Michaeli, I. Kleba, and J. Blaurock, *Polym. Eng. Sci.*, **42**, 846 (2002).
3. M. S. Gu, K. Chung, and J. R. Youn, *Polym. Eng. Sci.*, **41**(7), 1176 (2001).
4. C. Kim and J. R. Youn, *Polym-Plast. Technol.*, **39**, 163 (2000).
5. H. Park and J. R. Youn, *Polym. Eng. Sci.*, **39**, 457 (1999).
6. H. J. Lee, M. S. Thesis, Seoul National University, Seoul, 2000.
7. D. S. Kim and C. W. Macosko, *Polym. Eng. Sci.*, **27**, 2205 (2000).
8. C. Prakash and S. V. Patankar, *Numer. Heat Transfer*, **8**, 259 (1985).
9. J. Kim, J. R. Youn, and J. C. Hyun, *Korea-Australia Rheol. J.*, **13**, 97 (2001).
10. S. W. Lee, J. R. Youn, and J. C. Hyun, *Mater. Res. Innov.*, **6**, 189 (2002).
11. S. W. Lee and J. R. Youn, *Macromol. Symp.*, **148**, 211 (1999).